Analysis of Microstructure Evolution in Quenching and Partitioning Automotive Sheet Steel

JOHN G. SPEER, E. DE MOOR, K.O. FINDLEY, D.K. MATLOCK, B.C. DE COOMAN, and D.V. EDMONDS

Extensive research efforts are underway globally to develop new steel microstructure concepts for high-strength sheet products, driven largely by the need for lightweight automotive structures in support of designs to enhance occupant safety and energy efficiency. One promising approach, involving the quenching and partitioning (Q&P) process, was introduced in the predecessor to this paper series, *Austenite Formation and Decomposition, 2003*.[1] Development of the Q&P process has continued through to the present, and the current status is highlighted in this article, along with some alternative approaches that are also receiving attention. Special emphasis is placed on the synthesis and interpretation of the fundamental phase transformation responses, perspectives related to alloying and processing, and the resulting microstructure and properties. Key mechanistic issues are discussed, including carbide formation and suppression, migration of the martensite/austenite interface, carbon partitioning, and partitioning kinetics.

DOI: 10.1007/s11661-011-0869-7

I. INTRODUCTION

HIGH-strength automotive sheet steels represent an important technology in efforts to create vehicles with improved fuel efficiency and occupant safety. These steels have evolved with new alloying and processing strategies to tailor microstructures containing various mixtures of ferrite, martensite, bainite, and retained austenite. In North America, terminology has evolved whereby low-alloy dual-phase (DP), martensitic, austenite-containing transformation-induced plasticity (TRIP), and complex phase (CP) steels are referred to as First Generation advanced high-strength steel (AHSS).[2] Implementation of these steels has increased substantially in the past few years. Figure 1(a) shows several envelopes of tensile property combinations for a range of mild steels and First Generation AHSS grades. The Second Generation AHSS family includes more highly alloyed products such as Mn-added twinning-induced plasticity (TWIP) and reduced density steels achieved through aluminum alloying. These second-generation steels (shown in the upper right of Figure 1(a)) provide enhanced properties, although their application potential may be more limited because of the economic considerations associated with increased alloying and related processing challenges. Consequently, Third Generation AHSS concepts are being pursued vigorously to identify lower alloy steels that achieve ultrahigh-strength properties in combination with formability that is sufficient for implementation in automotive production. Reduced alloying and lower cost are important considerations for these steels, relative to the second-generation steels.[2] Third Generation AHSS steels are presently at the conceptual or early developmental stage, and the specific property requirements are not yet established, although it is considered that an important gap exists between the first- and second-generation steels, representing the future opportunity regime introduced in Figure 1(a).

The authors examined strategies to develop suitable microstructures for next-generation steels. The results from simple composite models to predict the tensile instability for assumed mixtures of ferrite + martensite or (stable) austenite + martensite are overlaid in Figure 1(b). Mixtures of ferrite and higher strength martensite (or "ultrafine" ferrite) are attractive and represent a broad range of ferrite-based steels, whereas austenite + martensite combinations generate properties within the targeted third-generation property band. Thus, austenite is considered to be a necessary ingredient of next-generation approaches because of the important contributions of its inherent high work-hardening rate.[2,3]

Austenite stability is also understood to influence the properties,[4–6] and control of the specific transformation characteristics of austenite have received consideration in recent composite modeling studies.[6–8] For example, Figure 2(a) illustrates predicted uniform elongation/tensile strength combinations for ferrite + austenite mixtures, where the mechanical stability of the austenite is varied according to the hypothetical behaviors shown

JOHN G. SPEER, Professor, E. DE MOOR and K.O. FINDLEY, Assistant Professors, and D.K. MATLOCK, Professor, are with the Advanced Steel Processing and Products Research Center, Colorado School of Mines, Golden, CO 80401. Contact e-mail: jspeer@mines.edu B.C. DE COOMAN, Professor, is with the Graduate Institute of Ferrous Technology, Pohang University of Science and Technology, Pohang, Kyungbuk 790-784, Republic of Korea. D.V. EDMONDS, Professor, is with the Institute for Materials Research, University of Leeds, Leeds LS2 9JT, United Kingdom.

Manuscript submitted February 16, 2011.
Article published online September 15, 2011

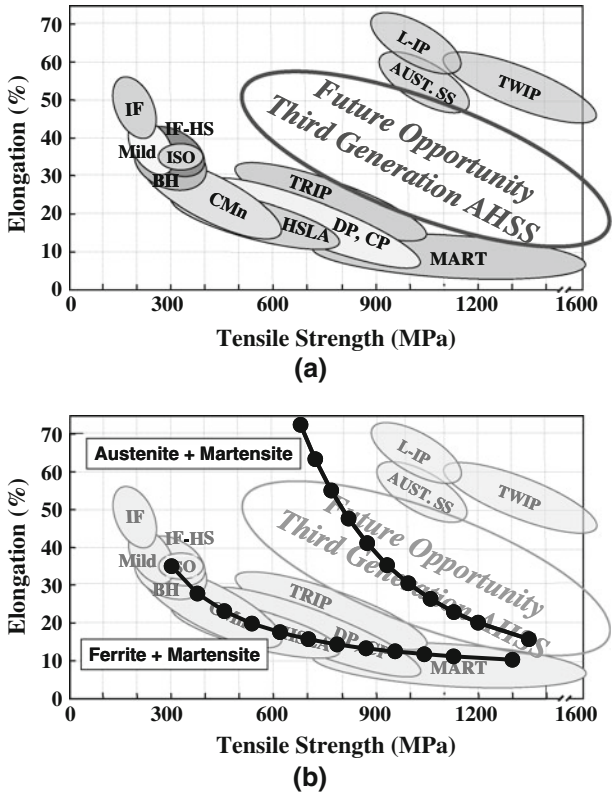

Fig. 1—Tensile elongation/strength combinations for various steel families, with (*a*) First Generation AHSS in the lower right, Second Generation AHSS in the upper right, and a wide region representing the opportunity for Third Generation AHSS. This figure is overlaid in (*b*) with property combinations predicted for various combinations of martensite and ferrite or (stable) austenite.[2]

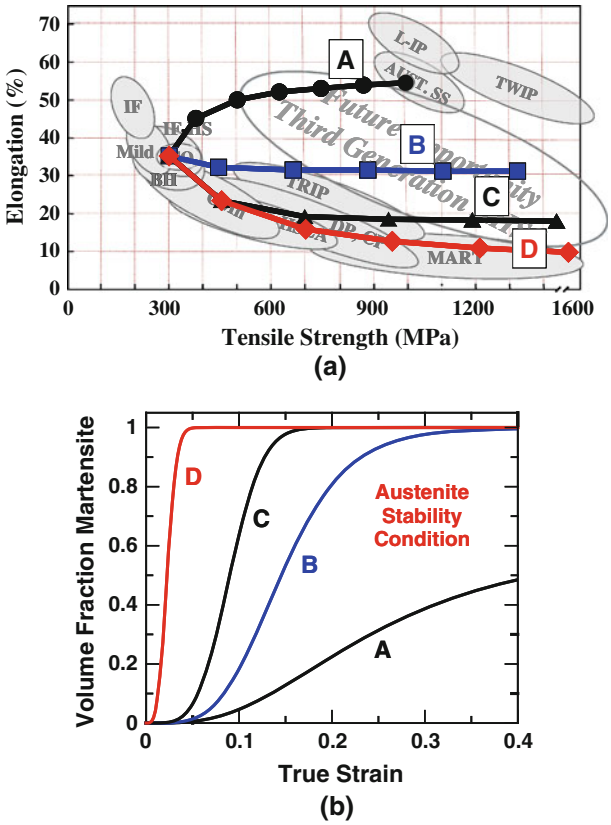

Fig. 2—Tensile ductility/strength combinations (*a*) for mixtures of martensite and metastable austenite, with austenite mechanical stability varying as shown in (*b*).[6]

in Figure 2(b).[6] As expected, unstable austenite (condition D) leads to properties similar to ferrite + martensite mixtures, but more importantly, new combinations of properties within the third-generation property band should become possible when the austenite fraction and stability can be controlled appropriately. Progress in tailoring the austenite behavior remains at an early stage, however. Austenite stabilization is controlled mostly by carbon enrichment to levels up to 1 pct or 2 pct (by weight), although manganese additions also have been employed also in early studies and are receiving revived attention in current research.[5,9–13]

The results of several promising approaches to generate high-strength austenite-containing microstructures are summarized in Figure 3.[7] Here, the total elongation is plotted for a variety of reported alloy/processing/microstructure combinations *vs* tensile strength. The reference curves (from Figure 1(b)) show calculated ranges for microstructures based on composite modeling of ferrite plus martensite (solid line) or stable austenite plus martensite (dashed line) mixtures, and the upper dashed line is within the range of properties desired for Third Generation AHSS. The studies summarized in Figure 3 include a variety of alloy/processing schemes aimed at generating high-strength, austenite-containing microstructures, plus two additional studies involving the refinement of dual-phase structures or special processing. Although sometimes ignored in the literature, tensile specimen geometry is well known to influence the measured value of total ductility. Hence, the data in Figure 3 are plotted after adjustment to account for differences in specimen geometry so that more meaningful comparisons may be made between the different investigations.[7,14] The figure shows that *several studies have yielded results plotting near or above the (calculated) dashed curve that is within the Third Generation AHSS property band.* Attractive data are represented particularly by some modified TRIP steels, carbide free bainites, and quench and partitioned steels (Q&P), with the Q&P steels being especially attractive at high strength levels.

The early "modified" TRIP steels involve higher carbon (~0.4 pct, compared with commercial grades typically containing approximately 0.2 pct carbon),[15] whereas some of the most exceptional Q&P steels also contain elevated levels of carbon (0.3 pct) and manganese (3 pct), or a different strategy with Ni/Cr additions and even higher carbon (0.4 pct).[10,16–18] Good properties have been reported by the nanobainite or "superbainite" approach using low-temperature austempering to accomplish microstructural refinement, although higher carbon levels and more extensive alloying may be involved also in these approaches.[3,19] Steels with "medium" manganese levels have received attention also, to reduce the alloying requirements in TWIP

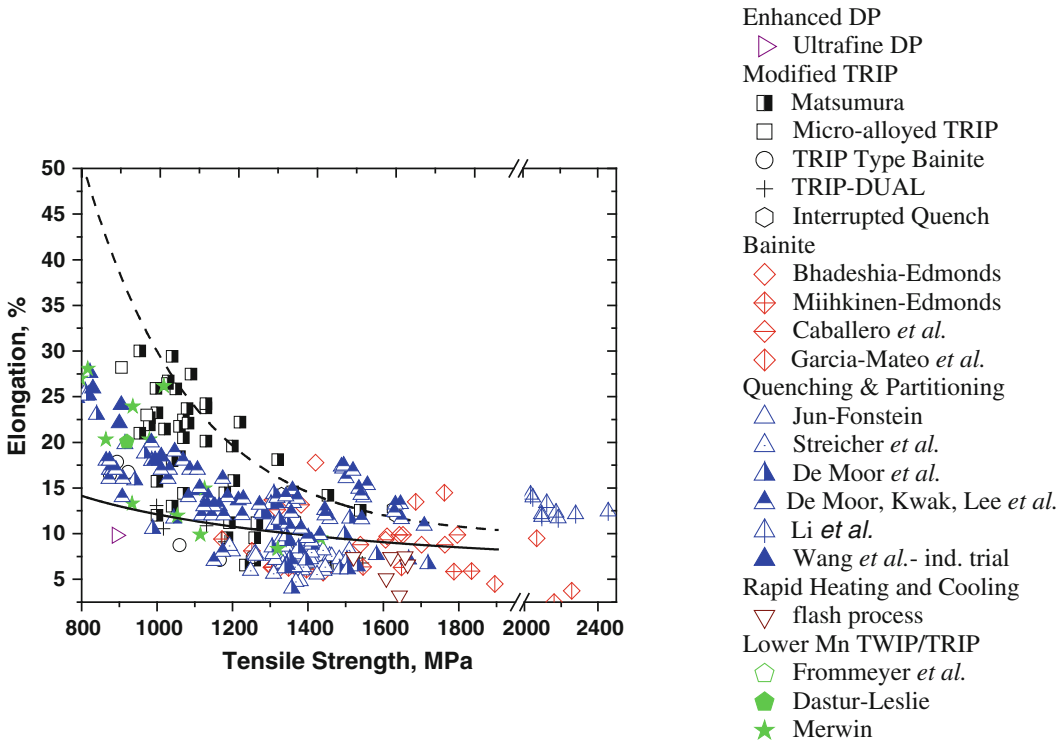

Fig. 3—Summary of total elongation and tensile strength combinations obtained by different metallurgical approaches (adjusted to ASTM E8 standard specimen geometry[7,14]). Estimated combinations of uniform elongation/tensile strength are also shown for selected martensite/ferrite (solid line) and martensite/austenite mixtures (dashed line) from Fig. 1(b). The cited studies are reviewed in Ref. 7.

products, or at lower levels (*e.g.,* 5 to 7 pct) to stabilize austenite in a fine duplex microstructure.[5,9]

The quenching and partitioning process was conceived by the authors, and early research was introduced in 2003 in *Austenite Formation and Decomposition,* the predecessor to this special article series.[1] The process has garnered increasing attention within the ferrous research community,[17,18,20–25] and industrial implementation efforts are underway.[24,25] The quenching and partitioning process is thus the focus of the text to follow. Some aspects of Q&P have been reviewed already as the research has progressed, and attention here is focused therefore on providing perspective on the current understanding of key fundamental questions that remain to be resolved in this actively evolving area.

II. QUENCHING AND PARTITIONING: BACKGROUND

Q&P is designed to create microstructures of martensite and retained austenite. The process concept involves an initial cooling step to a temperature between M_s and M_f to create controlled fractions of martensite and austenite, followed by a thermal treatment intended to promote carbon transport from supersaturated martensite into austenite, thereby stabilizing some of the austenite to room temperature. The original Q&P process signature is illustrated in Figure 4(a), where austenite is produced in an initial austenitizing or intercritical annealing treatment, followed by cooling to a carefully selected quenching temperature (QT), then followed by a partitioning treatment (time t at partitioning temperature, PT) that may consist of holding at the quenching temperature ("one step" Q&P), or at a higher temperature ("two-step" processing).[26] The Q&P process signatures in Figure 4(a) are considered applicable to the annealing of cold-rolled and coated sheet steel products, whereas nonisothermal partitioning has been explored more recently as a process route for rolled products that typically encounter continuous cooling conditions after rolling.[27,28] Figure 4(b) illustrates the concept for hot-strip mill product, where fast water cooling is available prior to coiling and subsequent slow cooling occurs in the wound coil. In this process configuration, the quenching and partitioning steps cannot be controlled independently because of intimate coupling between the processes whereby the coiling temperature serves to control the martensite fraction as well as the "initial" partitioning temperature (PT_i), *i.e.*, the thermal energy available in the coil to accomplish carbon partitioning.*

*Although the ability to apply the desired thermal process signature consistently raises important issues being considered in industrial scale-up investigations (related to microstructure and property variability), these engineering aspects are not addressed in this article.

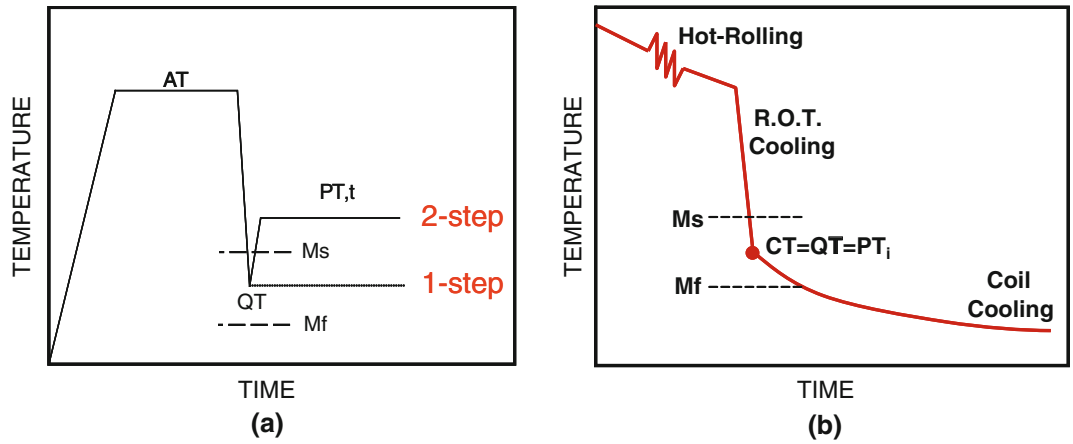

Fig. 4—Process schematic for one and two step Q&P processing (*a*). Nonisothermal Q&P concept (*b*) proposed for hot-rolled sheet steel processing.[27]

Q&P has also been considered in a hot stamping context related to the application of press hardened steels,[29] and recent experimental results are encouraging.[30]

The Q&P concept evolved out of observations that martensitic steels were sometimes found to contain retained austenite in amounts greater than expected, with the additional austenite stabilization hypothesized to arise from partitioning of carbon from supersaturated martensite. The Q&P process was conceived to use and control this behavior. The thermodynamic characteristics of carbon partitioning were then explored, with a possible endpoint of carbon partitioning defined as constrained carbon equilibrium (CCE) where carbon chemical potential gradients are eliminated under conditions where the austenite/martensite interface motion is constrained.[31–33] These early analyses confirmed that most of the carbon should preferentially reside in austenite[26,31] and led to an understanding of quench temperature sensitivity as shown in Figure 5. The figure shows calculated amounts of austenite (γ_{QT}) and martensite (M_{QT}) at the quench temperature prior to partitioning, and the final austenite fraction remaining (γ_{FINAL}), along with the amount of fresh martensite after full partitioning and final cooling to room temperature. The carbon concentration in the austenite (and fresh martensite) is given by C_γ. The knowledge provided by results such as illustrated in Figure 5 was critical to early experimental studies conducted to explore and develop the Q&P concept, as it provided guidance to quench temperature selection for specific steels, and understanding of the expected transformation behavior and microstructure characteristics. An ''optimum'' quench temperature was indicated by this model, where the amount of retained austenite would be maximized in the final product.

Some critical assumptions were embodied in the methodology associated with Figure 5, namely that (1) ideal carbon partitioning from martensite to austenite is completed, with virtually all of the carbon in the martensite being available to stabilize austenite; (2) the

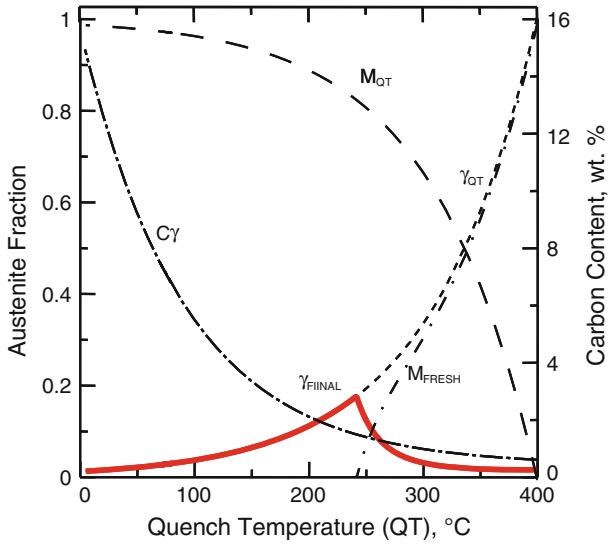

Fig. 5—Q&P processing diagram showing phase fractions and final austenite carbon concentration as a function of quenching temperature for a 0.19C-1.59Mn-1.63Si assuming ideal partitioning response.[26]

martensite and austenite fractions are unchanged during partitioning (implying stationary interfaces); and (3) competing processes such as carbide formation are suppressed completely. These assumptions have created discussion and occasional misunderstanding within the research community, and have generated some criticisms that have not been clearly voiced in the published literature to date, and so it is necessary and worthwhile to address these issues further.

In addition to carbon partitioning into austenite, other processes that could occur during the ''partitioning'' step are well known in martensite tempering. These processes include carbon trapping at dislocations and interfaces in the martensite, formation of carbides (both transition carbides and/or cementite), and decomposition of the austenite to bainite or other transformation products. Although little is known yet about the actual

migration of martensite/retained austenite interfaces during tempering, there can be a clear driving force for such processes,[34] which are suppressed only to the extent that the interface mobility is limited at the partitioning temperatures of interest. Thus, it should be understood that all the competing processes *may* be possible. To the extent that the modeled reactions are incomplete and the stated assumptions do not hold, then the simple model obviously does not provide a quantitatively accurate prediction. Some investigators have even suggested in unpublished commentary that the carbon partitioning mechanism is not supported by any experimental evidence. Many of the recent mechanistic studies associated with quenching and partitioning have thus aimed to understand these issues more completely.

III. ALLOY SELECTION AND MICROSTRUCTURE

Suppression of carbide formation was understood to be critical in early Q&P studies,[31] and silicon and/or aluminum were added at levels typical of TRIP sheet steels, where carbide-free bainitic microstructures with interlath retained austenite are obtained readily through austempering.[35] Early studies on silicon-containing steels showed that substantial austenite fractions could be stabilized via Q&P processing, and an important understanding of microstructure evolution was developed through the examination of Q&P processed AISI grade 9260, containing 0.6 pct C and 2 pct Si. The light optical micrograph in Figure 6 shows the presence of a substantial quantity of retained austenite, which is the white constituent (approximately 25 vol pct based on X-ray diffraction), interspersed with partitioned martensite, appearing more typical of a higher carbon microstructure that might be observed in a case-carburized steel.[36] Carbon enrichment of the austenite in this instance is believed to be a consequence of the partitioning mechanism operating in an effective manner at 673 K (400 °C). At a lower partitioning temperature of 523 K (250 °C) as shown in Figure 7(a), austenite stabilization is less effective, and extensive precipitation of transition carbides is noted.[37] The dark-field transmission electron micrograph in Figure 7(b), which was obtained using an austenite reflection, confirms the extensive austenite stabilization in this steel at the higher temperature of 673 K (400 °C). Austenite appears as thick films in combination with martensite laths. The difference in partitioning response between these two conditions is ascribed to strong suppression of cementite (which forms at higher temperature) by silicon and weak suppression of transition carbide (which forms at lower temperature). These behaviors are illustrated in the schematic precipitation-time-temperature curves for cementite and transition carbide in Figure 7(c).

More recently, the presence of fine carbides at low partitioning temperatures was incorporated into terminology used by some investigations to describe a quenching, partitioning, and tempering process variant,

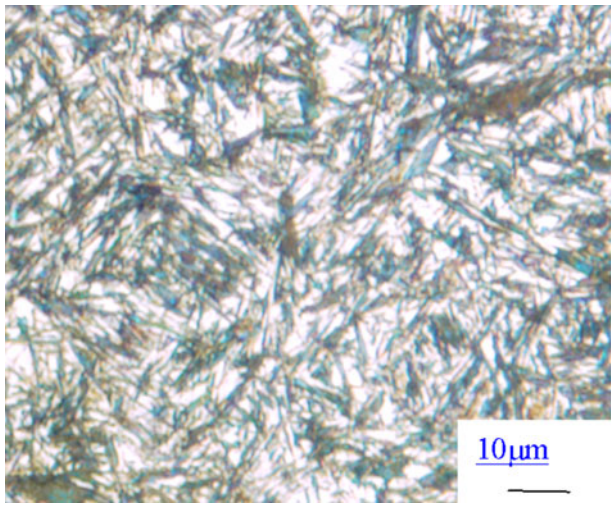

Fig. 6—Light optical micrograph of Q&P microstructure in AISI 9260 steel quenched to 463 K (190 °C) and partitioned at 673 K (400 °C).[36] Nital etch; retained austenite appears white.

acknowledging the beneficial[21,38] operation of classical tempering mechanisms in combination with partitioning at low temperatures.[37]** Because partitioning at higher temperatures usually involves first quenching to lower temperatures to provide sufficient martensite at the quenching step (*i.e.*, two-step processing), the potential for transition carbide precipitation at lower temperature, followed by dissolution during heating (above the transition carbide solvus) seems likely.[41] Nonetheless, the processes that occur during the quenching, thermal equilibration, and subsequent heating steps have not been characterized fully and remain a fruitful area for additional studies.

Although most Q&P studies have focused on Si-containing grades, aluminum additions have also been explored because of their ability to promote carbon enriched retained austenite in some bainitic TRIP steels.[41–43] (Like Si, Al and also Ni are graphitizing elements that have been found to stabilize transition carbides, suppressing cementite.[41]) Al is of particular interest in sheet steel applications because of its reduced tendency to form adherent oxides, which impact detrimentally surface quality and zinc coating wettability. Aluminum promotes bainite and has been found by different investigators to be less effective than silicon for stabilizing austenite in Q&P steels.[42,43] Molybdenum, in contrast, has been found to stabilize austenite effectively for longer times at higher partitioning temperatures, potentially of importance in hot-dip coated sheet products (where partitioning is accomplished in

**Substantial similarities also exist between (one-step) Q&P and some other processes proposed recently such as TRIP-dual,[23] Interrupted quenching plus tempering,[39] and TRIP aided bainitic ferrite.[40] These process variants incorporate a somewhat wider range of responses, including higher process temperatures where martensite formation is deemphasized and austempered carbide-free bainite is the primary constituent.

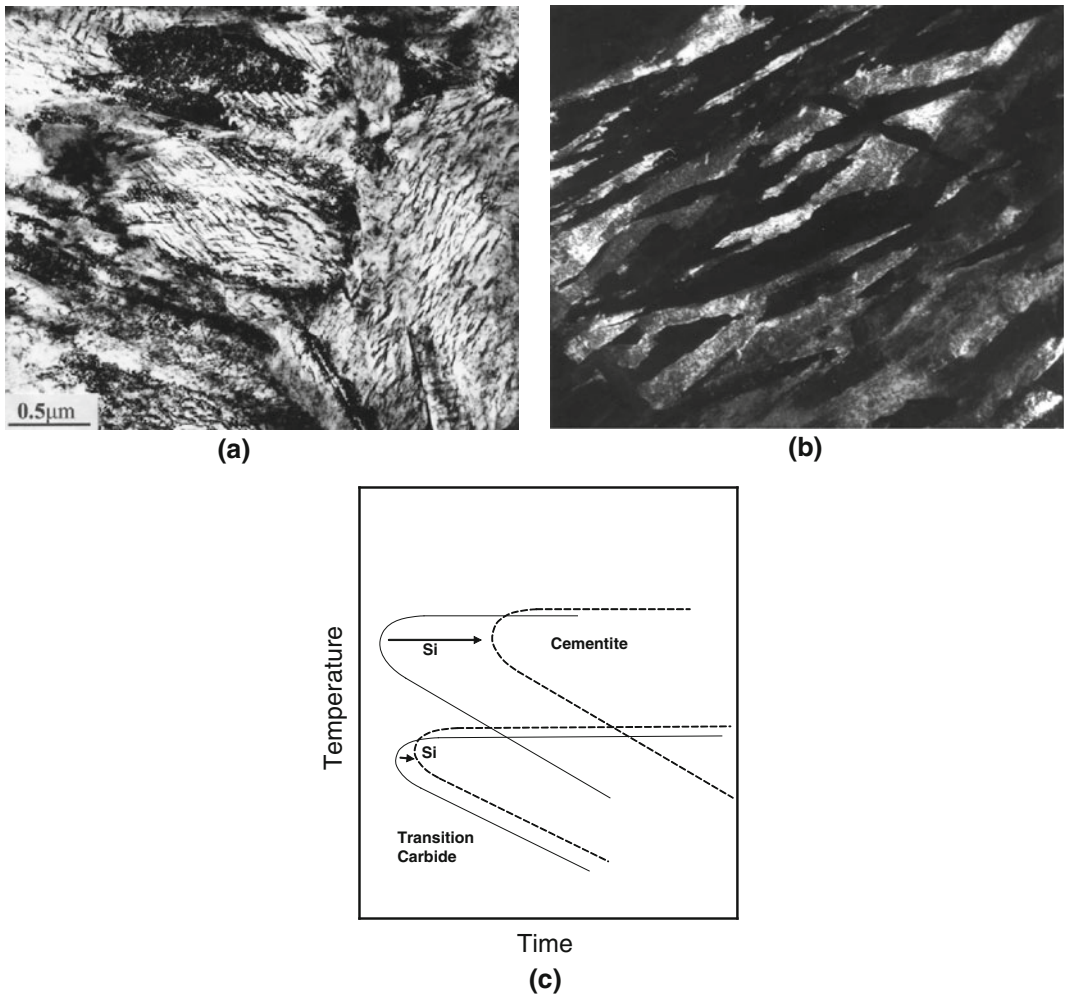

Fig. 7—Dark field TEM micrograph (*a*) of Q&P microstructure in AISI 9260 steel showing extensive transition carbide precipitation after quenching to 423 K (150 °C) and partitioning at 523 K (250 °C), and bright field TEM micrograph (*b*) at the same magnification showing austenite following quenching to 463 K (190 °C) and partitioning at 673 K (400 °C). Suggested effects of silicon on cementite and transition carbide precipitation kinetics are illustrated schematically in (*c*).[37]

conjunction with coating).[43] In this instance, the melting temperature of zinc necessitates a somewhat higher partitioning temperature than might otherwise be desired, such that greater suppression of austenite decomposition is important. Effective alloying approaches to suppress transition carbide precipitation (during low-temperature partitioning) and/or replace Si have not yet been identified, and experimental or *ab initio* studies could be useful in this regard.

IV. COMPETING PROCESSES AND KINETIC MODELS

Bainite has been recognized as a potential constituent in Q&P steels, particularly at increased quench temperatures where the amount of martensite is limited and the bainite transformation kinetics are more rapid than at a lower temperature. Some commentators have suggested in unpublished communications that bainite formation may be responsible for the austenite stabilization observed in Q&P processed microstructures. The correct interpretation of early microstructures in Q&P sheet steels (containing high levels of Al alloying) was also hindered by difficulties associated with distinguishing bainite from tempered martensite.[1] Nonetheless, the bainite kinetics can be suppressed readily by alloying[16] without substantially interfering with the Q&P response. A detailed analysis of the austenite stabilization occurring during Q&P processing was conducted by Clarke *et al*.[44] Figure 8 shows measured austenite fractions at room temperature as a function of quench temperature for four different partitioning times at 673 K (400 °C), along with the calculated austenite fractions assuming that the stabilization of austenite occurred instead via a carbide-free bainite transformation. Importantly, this analysis indicated that bainitic transformation was unable to account for the measured austenite fractions. Essentially, the transformation to carbide free bainite can stabilize significant fractions of the austenite in which it forms, but in usual Q&P processing, much of the initial austenite is transformed to martensite already during the initial quenching step. All the austenite that remains after quenching can (potentially) be stabilized

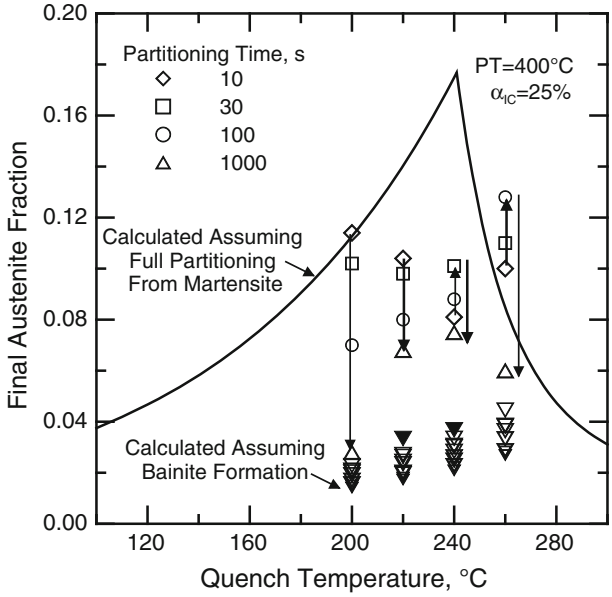

Fig. 8—Comparison of experimental austenite fractions (open symbols not including inverted triangles) and calculated austenite fractions assuming two different possible mechanisms for austenite stabilization. A calculated theoretical final austenite fraction curve is shown, based on an idealized full partitioning of carbon to austenite from martensite during Q&P processing. The austenite fractions (inverted triangles), which are calculated based on mass balance considerations assuming bainite formation, are also shown. The two solid points were calculated with carbon concentrations for both austenite and ferrite obtained using an atom probe, whereas the other austenite fractions were calculated using austenite carbon concentrations obtained from X-ray diffraction. PT = 673 K (400 °C) designates the partitioning temperature and α_{IC} designates the intercritical ferrite fraction.[44]

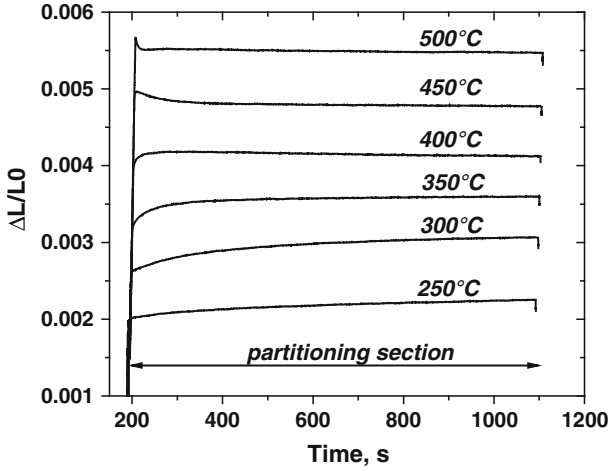

Fig. 9—Dilations measured during partitioning of a 0.24C, 1.61Mn, 1.45Si, and 0.3Al steel quenched to 523 K (250 °C).[43]

by a carbon partitioning mechanism, but *only a fraction* of the remaining austenite can be stabilized through bainite formation (where bainitic ferrite is the primary transformation product). Although bainite may *contribute* to austenite stabilization in some instances, the austenite fractions observed after Q&P processing necessitate the carbon partitioning mechanism to have been operative.[44]

The potential importance of interface migration during partitioning was noted previously. That is, if the martensite and austenite phase fractions developed during the quenching step are not fixed, then the final microstructure might be influenced as the partitioning step proceeds. Based on observed expansions identified using dilatometry, Kim *et al.*[45] first identified adjustments in the phase fractions during partitioning, through possible mechanisms such as isothermal martensite transformation, bainite formation, or interface migration. Figure 9 shows similar results, in this case incorporating a range of different partitioning temperatures for a fixed quench temperature. The kinetics are clearly faster at an increased temperature, but more interestingly, the expansions observed at lower partitioning temperatures are diminished as the partitioning temperature increases, and contractions are observed at 723 K and 773 K (450 °C and 500 °C).[43] This behavior is *qualitatively* consistent with a reversal in interface movement that might be expected[34,46] from ferrite growth at lower temperatures, to reduced ferrite growth, and eventually to austenite growth at higher temperature. The detailed mechanisms associated with these processes have not been identified and characterized clearly to date, although research is underway in an effort to understand these behaviors more accurately. Contractions were also observed during martensite tempering of this steel (after quenching to room temperature), and hence, it is not yet clear the extent to which the contraction relates to tempering effects or interface migration.

Early kinetic models of the partitioning process employed a stationary interface assumption,[47–49] using diffusion calculations using equal carbon potentials in the austenite and martensite at the interface. The kinetic models require assumptions related to the scale of the microstructure (diffusion distance) as well as the carbon mobility, and in general, the experimental partitioning times seem to be longer than would be predicted from the partitioning models. The models have thus far incorporated published values of carbon diffusivity in ferrite to represent carbon mobility in martensite and, hence, do not account for the influence of the martensite dislocation substructure on the carbon mobility (or chemical potential). Although there is some treatment of the thermodynamics of carbon trapping in the martensite tempering literature,[50] various thermodynamic and kinetic aspects of carbon migration in martensite are not quantified sufficiently at this time. The behavior during processing via Q&P is complicated even more by any precipitation of transitional carbides (and associated interactions with the scale of the microstructure[41]) and by temporal variation in the martensite defect structure during partitioning, associated with recovery processes. Several issues noted here have been scarcely considered, thus far, and additional data would be helpful.

The partitioning models were coupled with the previous martensite transformation models to predict the evolution of final austenite fractions under conditions where partitioning is not yet complete.[51] These models essentially applied the Koistinen-Marburger

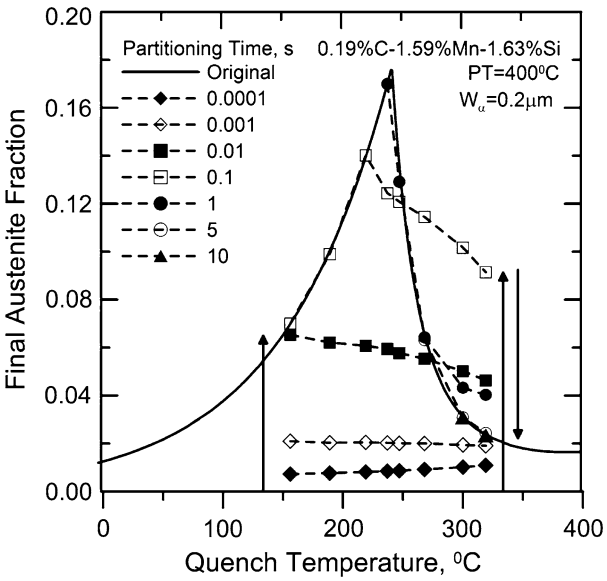

Fig. 10—Calculated final austenite fraction as a function of quench temperature for a 0.19C-1.59Mn-1.63Si alloy. Individual points that incorporate the kinetics of carbon partitioning are also shown for selected partitioning times. A ferrite width of $W_\alpha = 0.2\ \mu m$ was used for the partitioning temperature of 673K (400 °C). The arrows highlight austenite fraction behaviors with increasing partitioning time for quench temperatures above and below the optimum quench temperature.[51] A final austenite fraction curve (solid curve) is also shown that does not incorporate carbon partitioning kinetics but rather assumes complete ideal partitioning.

relationship on a local scale, in the presence of carbon concentration gradients in the austenite. An example is shown in Figure 10; generally, the results show the expected increase in austenite fraction as partitioning time increases early in the process and the eventual agreement with the values predicted assuming ideal partitioning. At intermediate times, however, some interesting behaviors are associated with the carbon gradients that develop during partitioning. At quench temperatures above the optimum temperature representing the peak in the theoretical curve, the amount of austenite after initial quenching is greater than the final amount that can be stabilized at room temperature. At these quench temperatures, it is apparent that the final austenite fraction is maximized at intermediate values of partitioning time, and then it decreases at longer times, indicating that greater austenite fractions may be possible than predicted under ideal partitioning conditions. (In fact, the *experimental* results shown in Figure 8 also exhibit this behavior.) The increased austenite associated with incomplete partitioning at high quench temperatures is a consequence of the greater austenite stability in the carbon-enriched regions of austenite when there is a composition gradient in the austenite, relative to the lower overall austenite stability when the carbon is distributed uniformly at a low level throughout a larger volume of austenite. It should be recognized that these models required simple assumptions about the austenite stability and martensite transformation behavior in the presence of local carbon concentration gradients that may be substantial relative

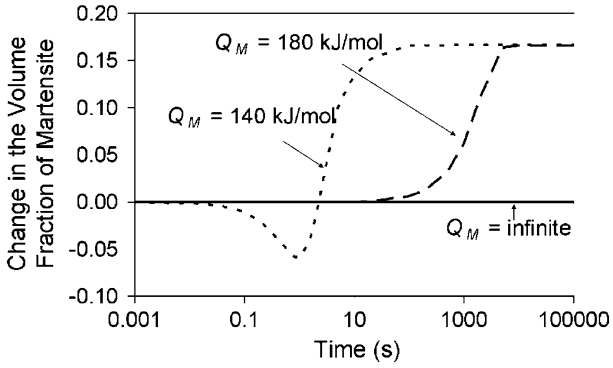

Fig. 11—Changes in the martensite fraction during partitioning, calculated based on three assumed values of the activation energy (Q_M) for migration of the martensite/austenite interface. The example was calculated for a 0.19C, 1.59Mn 1.63 Si steel, quenched to 573K (300 °C) and partitioned at 623 K (350 °C) for a 0.2 μm martensite lath width.[46]

to the dimensional scale of the martensite transformation product. Subsequent characterization and understanding of the "local austenite stability" and transformation behavior under these conditions is needed.

The kinetic models were extended later in studies by Santofimia *et al.*[46,52] to incorporate interface mobility, thus addressing the coupling between interface migration and carbon partitioning. The interface mobility is not well quantified, so different values were incorporated into the models with profoundly different implications. One example from this work is shown in Figure 11, which is calculated using three assumed values of the activation energy for interface migration. The implications of the models are discussed in greater detail elsewhere in this issue.[53] In Figure 11, the predicted movement of the martensite/austenite interface is reflected through changes in the martensite volume fraction, which are shown as a function of partitioning time at 623 K (350 °C) following quenching to 573 K (300 °C). Corresponding changes in the austenite fraction would be of equal magnitude and opposite sign. One activation energy was selected to represent an immobile interface ($Q_M = \infty$), and the other two were selected based on a review of the literature to reflect migration of an incoherent ferrite/austenite interface (Q_M = 140 kJ mol^{-1}) or a semicoherent ferrite/austenite interface (Q_M = 180 kJ mol^{-1}).[†] The results in the figure clearly confirm

[†]One might envision that a glissile austenite/martensite interface could have potentially even greater mobility,[54] but this situation has not yet been explored.

the possibility under some conditions that the transformation interface might move in one direction, and then reverse itself as a consequence of particular coupling between carbon partitioning and interface migration.[34,46,52] The endpoint of partitioning is also dependent on the assumptions made relative to interface mobility. If the interface is stationary, then partitioning

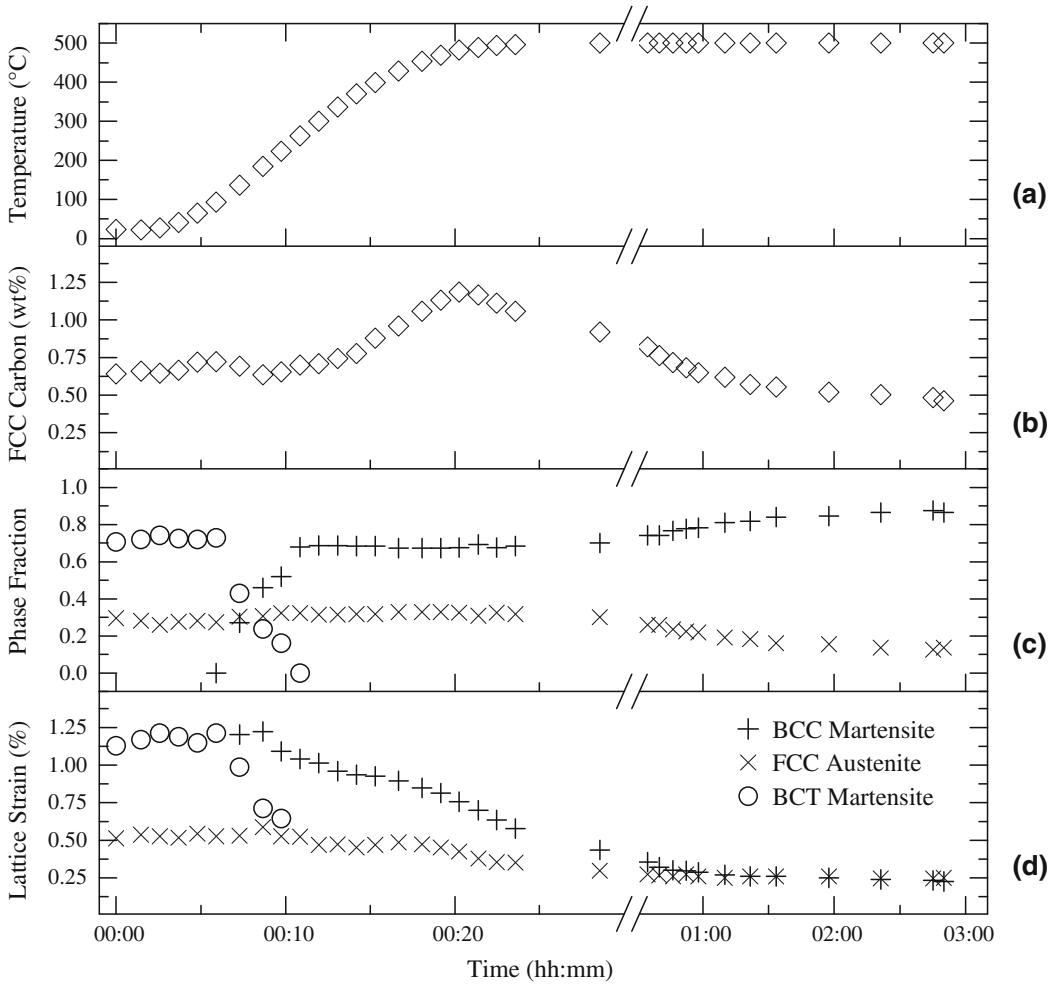

Fig. 12—*In situ* neutron diffraction results during heating (partitioning) of a 0.64C-4.57Mn-1.30Si steel after quenching to room temperature, showing phase fractions, austenite carbon concentration, and lattice strains.[56,57]

ends under constrained carbon equilibrium conditions, whereas a mobile interface would allow the phase fractions/compositions to adjust eventually to their metastable paraequilibrium values.[31,46] The interface mobility is, therefore, relevant from a microstructure design standpoint, as it influences both the volume fraction and the carbon concentration of the austenite resulting from Q&P processing.

Early thermodynamic predictions related to the end-point of carbon partitioning also suggested that high degrees or carbon enrichment may be possible, up to several weight percent of carbon in retained austenite.[31] The highest levels of carbon enrichment were expected in steels with lower austenite fractions. Although mechanical models (such as in Figure 2) point out the importance of austenite stabilization, the studies do not seem to have verified or exploited the high levels of austenite stabilization predicted by the early thermodynamic models. High levels of austenite enrichment have not yet been reported in low-alloy steels, and (average) austenite carbon concentrations are less than 2 wt pct. Nonetheless, massive carbon supersaturations have been reported in high-alloy austenite stainless steels.[55] As mentioned previously, a mobile interface would allow the phase compositions to adjust closer to their metastable paraequilibrium values. In this instance, the expected austenite carbon enrichment would not be consistent with the extreme levels predicted at "constrained carbon equilibrium," and subsequent exploration in this area could be both interesting and important.

V. ADDITIONAL EVIDENCE FOR CARBON PARTITIONING

Some fruitful efforts to verify the carbon partitioning mechanism have been completed recently, and Figure 12 shows the results of *in situ* neutron diffraction measurements made during heating (*i.e.*, partitioning) of a 0.64C-4.57Mn-1.30Si steel after quenching.[56] The high Mn level in this steel provided substantial austenite retention at ambient temperature prior to heating. The thermal profile is shown in Figure 12(a). The phase fraction results in Figure 12(c) indicate that the martensite tetragonality is eliminated early, and the phase

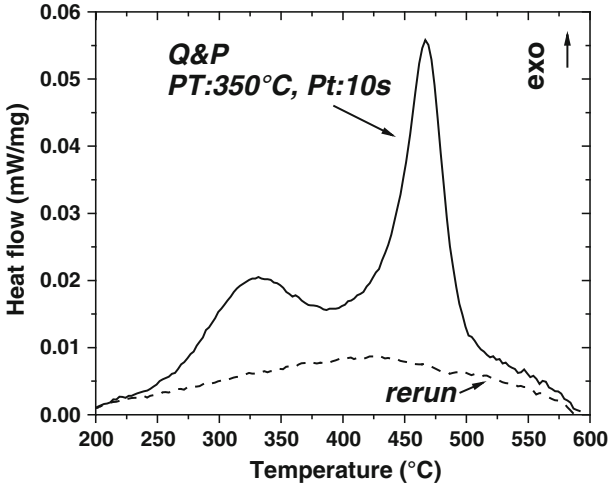

Fig. 13—Exothermic heat flow measured by differential scanning calorimetry for a 0.20C-1.63Mn-1.63Si steel measured during heating after Q&P processing involving quenching to 513 K (240 °C) and partitioning for 10s at 623 K (350 °C). The Q&P sample contained ~6 pct austenite prior to heating; the dashed curve involved a subsequent rerun of the sample after completion of partitioning and decomposition of the austenite[60].

fractions are essentially unchanged at intermediate times, whereas a substantial increase in the austenite carbon concentration is noted (Figure 12(b)), to a level in excess of 1 wt pct. (A corresponding depletion of carbon in the body-centered cubic (bcc) ferrite was also noted.[57]) These results provide *direct evidence of carbon partitioning* in the absence of any bainite formation.‡

‡The characteristic behaviors in the figure are different than observed in similar work involving bainite transformation, and bainite formation would clearly be accompanied by an increase in the bcc fraction and a decrease in the face-centered cubic fraction.[58]

Decomposition and carbon depletion of austenite are noted at longer times at elevated temperature, presumably associated with cementite formation. Interestingly, the lattice strain data (Figure 12(d)) suggest that recovery of the martensite is underway during the partitioning process.

In addition to the neutron diffraction results presented previously, recent atom probe data[59] and numerous X-ray diffraction results indicating austenite stabilization and carbon enrichment during partitioning in martensite/austenite mixtures,[26,36] differential scanning calorimetry (DSC) results are also consistent with the occurrence of carbon partitioning. The results in Figure 13 show the DSC signal during heating at 15 K/min for a 0.2C, 1.63Mn, and 1.63 Si steel Q&P processed by quenching to 513 K (240 °C) before partitioning 10 seconds at 623 K (350 °C) and then cooling to room temperature.[60] The specimen contained approximately 6 pct retained austenite prior to heating for DSC. Two DSC peaks were observed during heating (partitioning), and were absent upon rerunning of the same sample. The first peak was associated with heat released due to carbon partitioning. Importantly, the peak height was consistent with the enthalpy changes expected from partitioning, and the activation energy suggested carbon diffusion in ferrite. The second peak was associated with decomposition of the retained austenite, with the expected activation energy.

VI. CONCLUDING REMARKS

New perspectives have been provided in this article, focusing on recent advances in the understanding of microstructure evolution during the quenching and partitioning process, in a framework related to next-generation, advanced, high-strength automotive sheet steels containing retained austenite. Characterization and modeling have advanced considerably the understanding of Q&P steels during the past few years, and operation of the carbon partitioning mechanism now seems to be well supported, while much remains to be learned about specific details related to additional or competing mechanisms that can operate under some conditions. The Q&P process is receiving considerable attention in the ferrous research and development community. Many fundamental and practical questions remain, and some key research directions have been identified in this article, which would extend understanding and enable improved modeling.

ACKNOWLEDGMENTS

The authors gratefully acknowledge the sponsors of the Advanced Steel Processing and Products Research Center, an industry/university cooperative research center at the Colorado School of Mines, and the National Science Foundation through award number CMMI-0729114.

REFERENCES

1. J.G. Speer, A.M. Streicher, D.K. Matlock, F. Rizzo, and G. Krauss: *Austenite Formation and Decomposition*, ISS/TMS, Warrendale, PA, 2003, pp. 505–22.
2. D.K. Matlock and J.G. Speer: *Proc. of the 3rd International Conference on Structural Steels*, Korean Institute of Metals and Materials, Seoul, South Korea, 2006, pp. 774–81.
3. O. Kwon, K. Lee, G. Kim, and K.G. Chin: *Mater. Sci. Forum*, 2010, vol. 638-42, pp. 136–41.
4. M.L. Brandt and G.B. Olson: *Iron Steelmaker*, 1993, vol. 20 (5), pp. 55–60.
5. P. Gibbs, E. De Moor, M. Merwin, B. Clausen, J.G. Speer, and D.K. Matlock: *Metall. Mater. Trans. A*, DOI:10.1007/s11661-011-0687-y.
6. D.K. Matlock and J.G. Speer: *Microstructure and Texture in Steels and Other Materials*, Springer, London, UK, 2009, pp. 185–205.
7. E. De Moor, P.J. Gibbs, J.G. Speer, D.K. Matlock, and J.G. Schroth: *AIST Trans.*, 2010, vol. 7 (3), pp. 133–44.
8. H.N. Han, C.S. Oh, G. Kim, and O. Kwon: *Mater. Sci. Eng. A*, 2009, vol. A499, pp. 462–68.
9. M.J. Merwin: *Mater. Sci. Forum*, 2007, vol. 539-43, pp. 4327–32.
10. E. De Moor, D.K. Matlock, J.G. Speer, and M.J. Merwin: *Scripta Mater.*, 2011, vol. 64, pp. 185–88.
11. E. De Moor, J.G. Speer, D.K. Matlock, J.H. Kwak, and S.B. Lee: *ISIJ Int.*, 2011, vol. 51 (1), pp. 137–44.
12. S. Lee, K. Lee, and B.C. De Cooman: *Mater. Sci. Forum*, 2010, vol. 654-56, pp. 286–89.

13. J. Shi, X. Sun, M. Wang, W. Hui, H. Dong, and W. Cao: *Scripta Mater*., 2010, vol. 63, pp. 815–18.
14. ISO 2566/1-1984(E): *Steel—Conversion of Elongation Values – Part 1: Carbon and Low Alloy Steels*, 1984, pp. 1–28.
15. O. Matsumura, Y. Sakuma, and H. Takechi: *Trans. ISIJ*, 1987, vol. 27, pp. 570–79.
16. F. Rizzo, A.R. Martins, J.G. Speer, D. Matlock, A. Streicher, and B. De Cooman: *Mater. Sci. Forum*, 2007, vols. 539–543, pp. 4476–81.
17. H.Y. Li, X.W. Lu, W.J. Li, and X.J. Jin: *Metall. Mater. Trans. A*, 2010, vol. 41A, pp. 1284–1300.
18. M.J. Santofimia, T. Nguyen-Minh, L. Zhao, R. Petrov, I. Sabirov, and J. Sietsma: *Mater. Sci. Eng. A*, 2010, vol. A527, pp. 6429–39.
19. F.G. Caballero and H.K.D.H. Bhadeshia: *Curr. Opin. Solid State Mater. Sci*., 2004, vol. 8, pp. 251–57.
20. H.Y. Li, X.W. Lu, X.C. Wu, Y.A. Min, and X.J. Jin: *Mater. Sci. Eng. A*, 2010, vol. A527, pp. 6255–59.
21. N. Zhong, X.D. Wang, L. Wang, and Y.H. Rong: *Mater. Sci. Eng*., 2009, vol. 506, pp. 111–16.
22. H. Li and X. Jin: *Chin. J. Mech. Eng*., 2009, vol. 22, pp. 645–50.
23. H.J. Jun and N. Fonstein: *Proc. Intl. Conf. on New Developments in Advanced High-Strength Sheet Steels*, AIST, Warrendale, PA, 2008, pp. 155–68.
24. L. Wang and W. Feng: *Advanced Steels*, Springer-Verlag, New York, NY, 2011, pp. 255–58.
25. K.H. Kim: Patent Application WO2008KR7356A, 2008.
26. A.M. Streicher, J.G. Speer, D.K. Matlock, and B.C. De Cooman: *Int. Conf. on Advanced High-Strength Sheet Steels for Automotive Applications Proceedings*, AIST, Warrendale, PA, 2004, pp. 51–62.
27. G.A. Thomas, J.G. Speer, and D.K. Matlock: *AIST Trans*., 2008, vol. 5 (10), pp. 209–17.
28. G.A. Thomas, J.G. Speer, and D.K. Matlock: *Metall. Mater. Trans. A*, DOI:10.1007/s11661-011-0648-5.
29. M. Blankenau and R. Hughes: Private communication, June 9, 2004.
30. H. Liu, X. Lu, X. Jin, H. Dong, and J. Shi: *Scripta Mater*., 2011, vol. 64, pp. 749–52.
31. J.G. Speer, D.K. Matlock, B.C. De Cooman, and J.G. Schroth: *Acta Mater*., 2003, vol. 51, pp. 2611–22.
32. J.G. Speer, D.K. Matlock, B.C. De Cooman, and J.G. Schroth: *Scripta Mater*., 2005, vol. 52, pp. 83–85.
33. M. Hillert and J. Ågren: *Scripta Mater*., 2004, vol. 50, pp. 697–99.
34. J.G. Speer, R.E. Hackenberg, B.C. De Cooman, and D.K. Matlock: *Phil. Mag. Lett*, 2007, vol. 87, pp. 379–82.
35. M.F. Gallagher, J.G. Speer, D.K. Matlock, and N.M. Fonstein: *44th Mechanical Working and Steel Processing Conference Proc*., 2002, Vol. XL, pp. 153–72.
36. F.L.H. Gerdemann, J.G. Speer, and D.K. Matlock: *Proc. Materials Science and Technology 2004*, TMS/AIST, Warrendale, PA, 2004, pp. 439–49.
37. D.V. Edmonds, K. He, F.C. Rizzo, B.C. De Cooman, D.K. Matlock, and J.G. Speer: *Mater. Sci. Eng. A*, 2006, vols. A438–440, pp. 25–34.
38. A.J. Shutts, J.G. Speer, D.K. Matlock, D.V. Edmonds, F. Rizzo, and E.B. Damm: *Int. Conf. on New Developments in Long and Forged Products: Metallurgy and Applications*, AIST, Warrendale, PA, 2006, pp. 191–202.
39. S. Cobo, C. Colin, and S. Allain: *New Developments on Metallurgy and Applications of High Strength Steels*, vol. 1, TMS, Warrendale, PA, 2008, pp. 209–21.
40. K. Sugimoto, M. Murata, and S.M. Song: *ISIJ Int*., 2010, vol. 50, pp. 162–68.
41. D.V. Edmonds, K. He, F.C. Rizzo, J.G. Speer, and D.K. Matlock: *New Developments on Metallurgy and Applications of High Strength Steels*, vol. 2, TMS, Warrendale, PA, 2008, pp. 829–41.
42. M.J. Santofimia, T. Nguyen-Minh, L. Zhao, D.N. Hanlon, T.A. Kop, and J. Sietsma: *Proc. of the Intl. Conf. on New Developments in Advanced High-Strength Sheet Steels*, AIST, Warrendale, PA, 2008, pp. 191–98.
43. E. De Moor, J. Penning, C. Föjer, A.J. Clarke, and J.G. Speer: *Proc. of the Intl. Conf. on New Developments in Advanced High-Strength Sheet Steels*, AIST, Warrendale, PA, 2008, pp. 199–207.
44. A.J. Clarke, J.G. Speer, M.K. Miller, R.E. Hackenberg, D.V. Edmonds, D.K. Matlock, F.C. Rizzo, K.D. Clarke, and E. De Moor: *Acta Mater*., 2008, vol. 56, pp. 16–22.
45. D.H. Kim, J. Speer, H.S. Kim, and B. De Cooman: *Metall. Mater. Trans. A*, 2009, vol. 40A, pp. 2048–60.
46. M.J. Santofimia, J.G. Speer, A. Clarke, L. Zhao, and J. Sietsma: *Acta Mater*., 2009, vol. 57, pp. 4548–57.
47. M. Hillert, L. Hoglund, and J. Ågren: *Acta Metall. Mater*., 1993, vol. 41, pp. 1951–57.
48. F. Rizzo, D Edmonds, K. He, J. Speer, D. Matlock, and A.M. Streicher: *Solid-to-Solid Phase Transformations in Inorganic Materials 2005*, vol. 1, TMS, Warrendale, PA, 2005, pp. 535–44.
49. A. Clarke, J.G. Speer, D.K. Matlock, F.C. Rizzo, D.V. Edmonds, and K. He: *Solid-to-Solid Phase Transformations in Inorganic Materials 2005*, vol. 2, TMS, Warrendale, PA, 2005, pp. 99–108.
50. D. Kalish and M. Cohen: *Mater. Sci. Eng*., 1970, vol. 6, pp. 156–66.
51. A.J. Clarke, J.G. Speer, D.K. Matlock, F.C. Rizzo, D.V. Edmonds, and M.J. Santofimia: *Scripta Mater*., 2009, vol. 61, pp. 149–52.
52. M.J. Santofimia, L. Zhao, and J. Sietsma: *Scripta Mater*., 2008, vol. 59, pp. 159–62.
53. M.J. Santofimia, L. Zhao, and J. Sietsma: *Metall. Mater. Trans. A*, DOI:10.1007/s11661-011-0706-z.
54. G.R. Purdy: Personal communication, May 11, 2011.
55. Y. Cao, F. Ernst, and G.M. Michal: *Acta Mater*., 2003, vol. 51, pp. 4171–81.
56. T.D. Bigg, D.K. Matlock, J.G. Speer, and D.V. Edmonds: *Solid State Phenom*., 2011, vols. 172–174, pp. 827–32.
57. D.V. Edmonds, D.K. Matlock, and J.G. Speer: *Proc. 1st Int. Conf. Advanced Steels*, Metallurgical Industry Press, Beijing, China, 2010, pp. 229–41.
58. H.J. Stone, M.J. Peet, H.K.D.H. Bhadeshia, P.J. Withers, S.S. Babu, and E.D. Specht: *Proc. R. Soc. A*, 2008, vol. 464, pp. 1009–27.
59. F. Danoix: unpublished research, Universite de Rouen, 2011.
60. E. De Moor, C. Föjer, J. Penning, A.J. Clarke, and J.G. Speer: *Phys. Rev. B*, 2010, vol. 82, pp. 104210-1-5.